Available online at www.sciencedirect.com
ScienceDirect
Soils and Foundations 66 (2026) 101833
SOILS AND FOUNDATIONS
www.elsevier.com/locate/sandf

Technical Paper

Specimen configuration effect on interface characterization using element anchor

Genbao Zhang [a,b,c,*], Tianchong Feng [a,c], Jorge G. Zornberg [d], Changfu Chen [e], Haibin Ding [b,f], Junbo Sun [g], Shimin Zhu [h], Changjie Xu [b,f]

[a] *College of Civil Engineering, Hunan City University, Yiyang 413000, China*
[b] *School of Civil Engineering and Architecture, East China Jiao Tong University, Nanchang 330013, Jiangxi, China*
[c] *Hunan Engineering Research Center of Structural Safety and Disaster Prevention for Urban Underground Infrastructure, Yiyang, Hunan 413000, China*
[d] *Department of Civil, Architectural and Environmental Engineering, The University of Texas at Austin, TX 78712, USA*
[e] *College of Civil Engineering, Hunan University, Changsha. 410086, China*
[f] *State Key Laboratory of Safety and Resilience of Civil Engineering in Mountain Area, East China Jiaotong University, Nanchang 330013, China*
[g] *School of Design and Built Environment, Curtin University, Perth, WA 6102, Australia*
[h] *School of Civil Engineering, Ludong University, Yantai 264025, China*

Received 28 January 2026; received in revised form 9 June 2026; accepted 29 June 2026

Abstract

Pullout test of element anchor specimens have been increasingly adopted to characterize the interface behavior of ground anchors. The effect of the configuration conditions of element anchor specimens on their interface characterization were investigated combining the laboratory tests and numerical simulations. Forty-eight element anchor specimens, reinforced with rebar tendons, were prepared using multiple bond/free length ratios and tested using consistent loading modes to quantify interface shear. The peak average interface shear strength was almost insensitive to configuration conditions when the ratio between bond length and grout diameter exceeded 2.10 or the ratio between free length and grout diameter exceeded 0.53. Additionally, the normalized peak average interface shear strength measured in the interface characterization was found to grow linearly with the increasing free/bond length ratio of the specimen. An interface shear displacement zone with a spindle-shaped distribution was found to develop within the soil surrounding the element anchor specimens when reaching the peak interface shear strength. However, the soil deformation zone developed a uniform distribution along the entire interface once testing reached the residual shear phase. Use of the reserved anchorage method to achieve a consistent interface shear area was found to effectively improve the uniformity of interface shear displacement throughout the interface.

Keywords: Interface characterization; Element anchor specimen; Free/bond length ratio; Soil deformation; Interface shear displacement

1. Introduction

The characteristics of the interface shear of anchors govern the actual magnitude of the anchor's bearing capacity. Accordingly, an accurate bond-slip model of the anchorage interface (i.e., an adequate anchorage interface shear model) is necessary to produce reliable anchor design calculations (Ren et al., 2010; Martin et al., 2011; Ma et al., 2016; Zou and Zhang, 2019). Currently, two methods have

* Corresponding author at: College of Civil Engineering, Hunan City University, Yiyang 413000, China.

E-mail addresses: genbao@hncu.edu.cn (G. Zhang), ghs5562020@163.com (T. Feng), zornberg@mail.utexas.edu (J.G. Zornberg), cfchen@hnu.edu.cn (C. Chen), hbding@ecitu.edu.cn (H. Ding), tunneltc@gmail.com (J. Sun), smzhu@ldu.edu.cn (S. Zhu), xucj@zju.edu.cn (C. Xu).

https://doi.org/10.1016/j.sandf.2026.101833
0038-0806/

been primarily adopted to predict anchorage interface shear characteristics. The first method is a semi-empirical field approach, which involves conducting a back analysis using data collected from an in-situ pullout test of a full-scale anchor (Benmokrane et al., 1995; Cheng et al., 2016; Liu et al., 2017). The second method involves a laboratory approach in which the anchorage interface behavior is directly characterized through pullout testing of element anchor specimens (Chen et al., 2018, 2019, 2020; Zhang et al., 2020). While field method offers prototype-scale conditions, its results are subjected to often unknown subsurface and environmental conditions and implementation of a comprehensive program may be cost-prohibitive. On the other hand, the laboratory method facilitates the physical simulation of anchorage interfaces under well controlled conditions and enables cost-effectively testing of combinations of design variables. Actually, the element-scale shear test has been widely used to obtain the shear behavior of newly developed geomaterials (Chen et al., 2025) and varying interfaces between the underground structure and the ground (Li et al., 2024). Based on extensive data analysis, previous studies have applied the laboratory method to develop theoretical (Ma et al., 2016, Chen et al., 2022b, Han et al., 2022) or data-driven (Zhang et al., 2022a, 2022b, 2022c) bond-slip models as well as time-dependent rheological interface models (Chen et al., 2021, 2022a; Zhu et al., 2022) for different anchorage interfaces. However, results from the latter approach require careful consideration of the test configuration and scale considerations to make improvement of physical simulation for field conditions of the full-scale anchor (GB50086-2015, 2016).

The characterization of anchorage interfaces involves element specimen concepts (i.e., use of a specimen in element scale simulating a point in mechanical analyses) that have been widely adopted in laboratory testing of grouted anchors and rock bolts (Chen et al., 2019). This characterization involves assumptions such as stress–strain-homogenization over the interface, and the use of comparatively short anchors that are subjected to pullout loading. The resulting test data is suitable to develop or calibrate interface bond-slip models to simulate the pullout load and displacements applied at the anchor specimen head (Chen et al., 2018, 2020; Zhang et al., 2020). Consequently, the implementation of element specimen concepts is critical for such anchorage interface characterizations. However, the influence on test results induced by the specimen configurations for element anchor specimen, particularly the bond/free length ratio as well as the alternatives to maintaining the consistent interface shear area, have not been thoroughly investigated. This situation impedes the standardization of the testing protocols for characterization of the anchorage interface behavior in engineering practice.

In order to address the limitations identified for characterization of anchor interfaces using a laboratory method, this study presents the results of a comprehensive experimental testing program complemented with numerical modeling of the pullout test. The overall objective of the study is to investigate the influence on the interface characterization results brought from the varying configuration conditions of element anchor specimens when tested in the laboratory, which include specifically the bond/free length ratio of element anchor specimen and the alternatives maintaining the consistent interface shear area. In doing so, the study also provides indirect insight into the extent to which the actual shear displacement distribution approaches the idealized uniform state under different configurations, and clarifies the mechanism by which the free section contributes to the interface shear response. A total of 48 element anchor specimens with varying bond/free length ratios were prepared and tested as part of this study. In addition, numerical simulations of a typical pullout test on an element anchor specimen were carried out using different methods to achieve a consistent interface contact area. The study includes a thorough analysis of the pullout response of the element anchor specimens as well as the strain behavior of the soil shear bands that develop near the anchor interface in order to ultimately determine the optimal configuration conditions for testing element anchor specimens.

2. Pullout testing program of element anchor specimens with varying configurations

2.1. Testing program

A specially-designed system to characterize the interface frictional behavior of anchor elements was adopted in this study as part of the sample preparation and subsequent pullout testing. Specific details on the test device and testing protocols have previously been reported in the literature (Chen et al., 2019; Zhang et al., 2020). The test method follows a load-transfer analysis framework previously established by the authors for translating interface parameters from the element scale to the field scale (Chen et al., 2021, 2022a). It is noteworthy that the confining pressure of the element anchor specimen was not incorporated into the loading scheme for the test device used in this work. This design is justified by a previous investigation by the authors, which demonstrated that the ground pressure confining the anchor in practice is remarkably released during borehole drilling due to the soil arching effect around the anchor hole, and therefore has negligible influence on the interface shear behavior of the element anchor specimen (Chen and Zhu, 2024). Similar stress release induced by soil arching during borehole drilling has also been widely reported across different soil types, from soft clays to sandy soils (Wang et al., 2023; Li et al., 2021; Zhao et al., 2025; Liu et al., 2022). Consequently, the interface shear strength measured under the zero-confinement condition can be regarded as a baseline value for the anchor–soil interface. In practical anchor engineering, the confining pressure around the borehole gradually recovers after grouting, and the resulting frictional component can only increase rather than reduce the interface resistance; adopting this zero-confinement baseline value as a design reference is therefore conservative. Preparation of the element anchor specimens included placing the surrounding soils using a consistent target water content and dry density. The testing program involved element anchor specimens tested under different configurations, which were achieved by varying the bond/free length ratio of the different element anchors. The free section of the anchorage facilitates the use of a constant interface contact area without changing the size of the anchor element.

The element anchor specimens were inserted into an anchor hole with a diameter of 3.8 cm and were prepared adopting bond lengths ranging from 3 cm to 10 cm. It is noteworthy that the diameter ratio between the specimen and the anchor hole is specially set to be 22/3.8 (i.e., 5.8), which exceeds the diameter ratio threshold of 5 established in a previous investigation by the authors (Chen and Zhu, 2024). That study demonstrated that, under unconfined conditions, when the diameter ratio between the specimen and the anchorage body exceeds 5, the influence of boundary conditions on the interface shear behavior can be eliminated. Therefore, the diameter ratio of 5.8 adopted in this study is sufficient to eliminate boundary effects for the tested clay, and the effect of boundary conditions can be considered negligible. The free length of the anchor elements was varied from 2 cm to 7 cm, a range that was determined based on the pullout displacement limit (2 cm) of the loading device. A 1-cm-thick plexiglass stopper was placed at the bottom of the anchor hole to facilitate tendon alignment and the leak-tightness of cement mortar, resulting in a total specimen length ranging from 6 cm to 18 cm. The range of bond length and free length when normalized to the diameter of grouting hole is 0.79 to 2.63, and 0.53 to 1.84, ensuring the specimen short enough (normalized full length range of 1.58–4.73) to be an element comparing with the prototype-scale anchor (normalized full length range of 30–100) (Benmokrane et al., 1995; Chen et al., 2019). Fig. 1 presents the schematic view of an element anchor specimen, illustrating its bond and free sections, which were varied to achieve anchor elements prepared using different bond/free ratios. The various bond and free length combinations adopted in this study are shown in Table 1. Additionally, each specimen can be named using the combination of bond/free length in Table 1 to facilitate the following descriptions, e.g., specimen b3u3 corresponds to the specimen with bond length of 3 cm and free length of 3 cm. Specimens were organized into eight testing groups characterized by a specific bond length. The anchor elements tested in each group were in turn prepared using six different free lengths.

2.2. Testing materials

Table 2 summarizes the properties for the various materials used in the testing program conducted in this study. The clay samples were collected from the floodplains near the Xiangjiang River in the City of Changsha, China. After the removal of impurities and oven-drying, the clay samples were sieved under 5 mm in order to use this material as surrounding soils for the element anchor specimens. The physical and mechanical properties of the clay samples were experimentally obtained as part of this study. The gradation curve of the clay soil is shown in Fig. 2. Cement mortar prepared using a water-cement ratio of 0.45 was used to grout the anchor hole. The density of the surrounding soils for all specimens were consistently used at 1.5 g/cm3 with the consistent moisture content at 18%. Rear tendons of HRB 400 were used as reinforcement. The details of specimen preparation can be referred to the previously published work (Chen et al., 2019; Zhang et al., 2020).

3. Pullout test results

All the tested specimens experienced the shear failure at the interface between the grout and the surrounding soils.

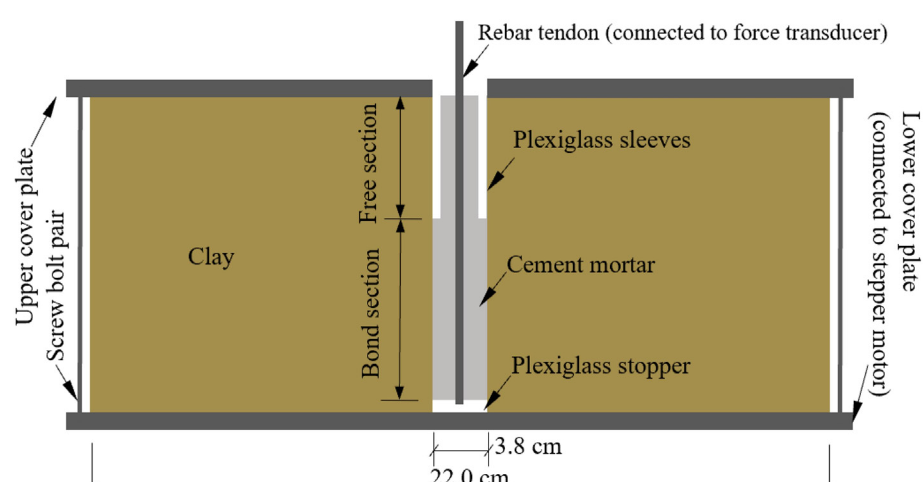

Fig. 1. Schematic of an element anchor specimen prepared using bond and free sections selected to achieve a target free/bond ratio.

Table 1
Combinations of different bond/free length ratios of element anchor specimens tested in this study.

Bond length (cm)	**Free length (cm)**					
	2	**3**	**4**	**5**	**6**	**7**
3	b3u2	b3u3	b3u4	b3u5	b3u6	b3u7
4	b4u2	b4u3	b4u4	b4u5	b4u6	b4u7
5	b5u2	b5u3	b5u4	b5u5	b5u6	b5u7
6	b6u2	b6u3	b6u4	b6u5	b6u6	b6u7
7	b7u2	b7u3	b7u4	b7u5	b7u6	b7u7
8	b8u2	b8u3	b8u4	b8u5	b8u6	b8u7
9	b9u2	b9u3	b9u4	b9u5	b9u6	b9u7
10	b10u2	b10u3	b10u4	b10u5	b10u6	b10u7

Table 2
Properties of materials used in the testing program.

Properties	Values/Description
Clay soil	
Specific gravity	2.69
Plastic limit (%)	20.9
Liquid limit (%)	36.8
Controlled dry density (g/cm^3)	1.5
Controlled moisture content (%)	18
Nonuniformity coefficient C_u	3.75
Coefficient of curvature C_c	0.42
Cohesion (kPa)	24.5
Internal friction angle (°)	38.7
Cement mortar	
Sand type	Medium sand
Cement type	P.O 42.5
Water/cement ratio (%)	45
Grouting method	Gravity
Diameter of grouting hole (cm)	3.8
Reinforcement	
Tendon type	Rebar of HRB 400
Diameter (mm)	8
Tensile strength (MPa)	460
Elastic modulus (GPa)	40
Yield strength (MPa)	380

The pullout responses (i.e., pullout force–displacement curves) for each group of specimens are presented in Fig. 3. The characteristic points in each pullout responses were identified using the peak and the residual values of the pullout forces as schematically shown in Fig. 4. The information deduced from the characteristic points corresponding to different specimen groups were presented in Table 3.

3.1. Free length-induced soil confinement

It is noteworthy that the pullout responses are supposed to be in a similar pattern for the specimens with the same bond length. However, it is observed in Fig. 3 that the free length of the element anchor specimen significantly affects the pullout response. As seen in Fig. 5, the increase of free length can lead to the increasing peak pullout force for the specimens with the same bond length with the increase amplitude ranging from 25.1% (for b = 8 cm) to 81.2% (for b = 3 cm). This trend indicates that the bond length of 8 cm (i.e., of 2.10 normalized to grouting hole diameter) attains the best insensitivity to the free length variation, and this value can be regarded as an empirical reference threshold derived from the materials tested in this study. Its applicability to other soil types or grouting materials remains to be further verified.

The confinement caused by the soils in free section (Fig. 1) can be used to explain the free length difference induced increase of the peak interface shear strength. The shear band developed in the surrounding soil along the interface, which would be resisted by the soil confinement. In the perspective of energy dissipation, the interface shear is accompanied with the soil deformation, of which both consumes the energy applied by the pullout force. The thicker free section overburdening

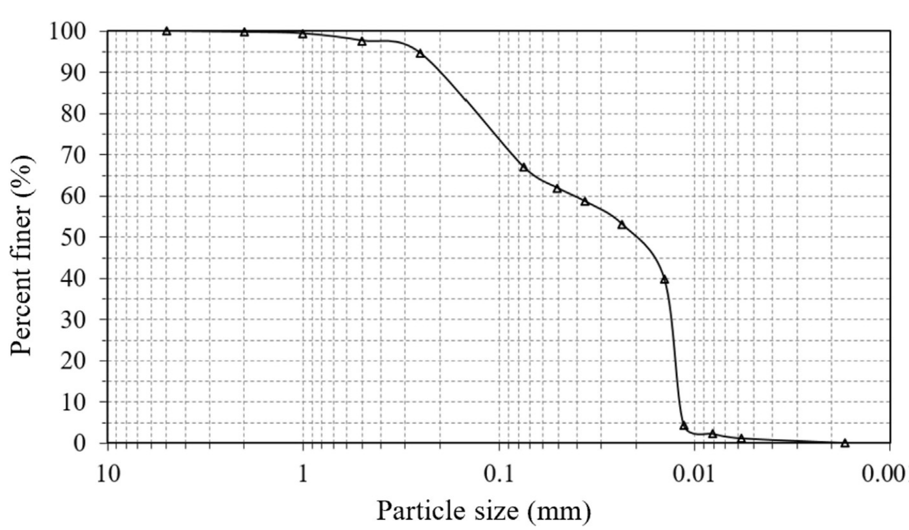

Fig. 2. Particle size distribution of the clay soil used in the testing program.

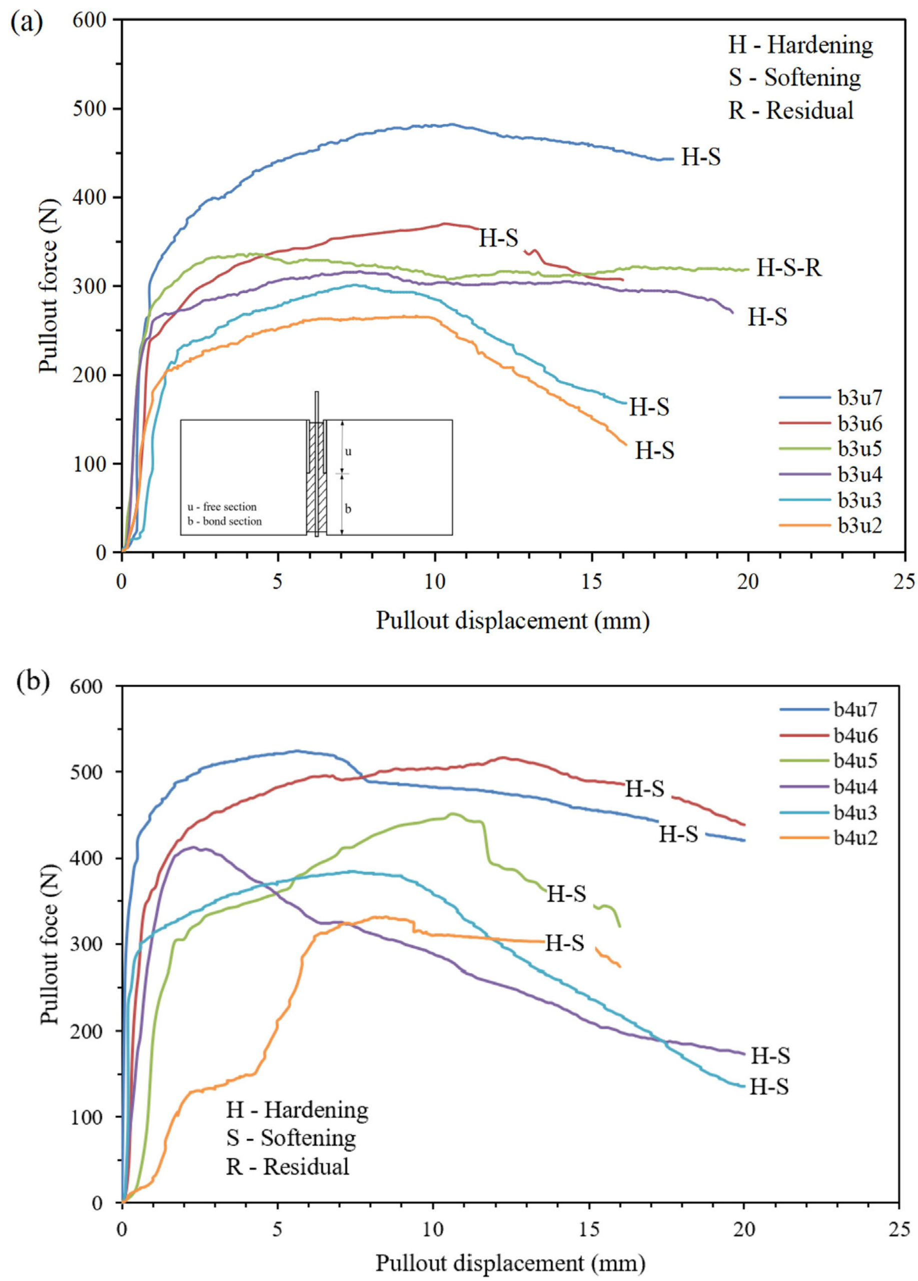

Fig. 3. Pullout response of element anchor specimens prepared using different bond lengths: (a) 3 cm; (b) 4 cm; (c) 5 cm; (d) 6 cm; (e) 7 cm; (f) 8 cm; (g) 9 cm; and (h) 10 cm. (Note: H-S-R indicates the pullout response manifested by hardening–softening-residual phase, while H-S by hardening–softening phase).

the shear band results in the greater energy consumption, which corresponding to the greater interface shear strength. In terms of mechanical roles, the free section transmits only axial tensile stress, whereas the bond section sustains both axial tensile stress and interface shear stress. Hence, the confinement provided by the free section does not originate from its own bond resistance, but rather from the passive restraint exerted by the overburdening soil against the shear deformation in the bond zone. A longer free section means a thicker overburden, which intensifies this passive restraint and leads to a higher peak interface shear strength.

3.2. Bound value of free/bond length ratio

Fig. 6 presents the softening rate of pullout response (manifested by the descending rate of pullout force over the increasing pullout displacement as seen in Fig. 4) versus the u/b (the ratio between the free length and bond length) for the specimen group with the same bond length. It is observed that the softening rate of the specimens was remarkably affected by the u/b.

Observations upon the trend of softening rate at different value of the u/b, a bound value can be found appropriately at the value of 1, as demonstrated by the

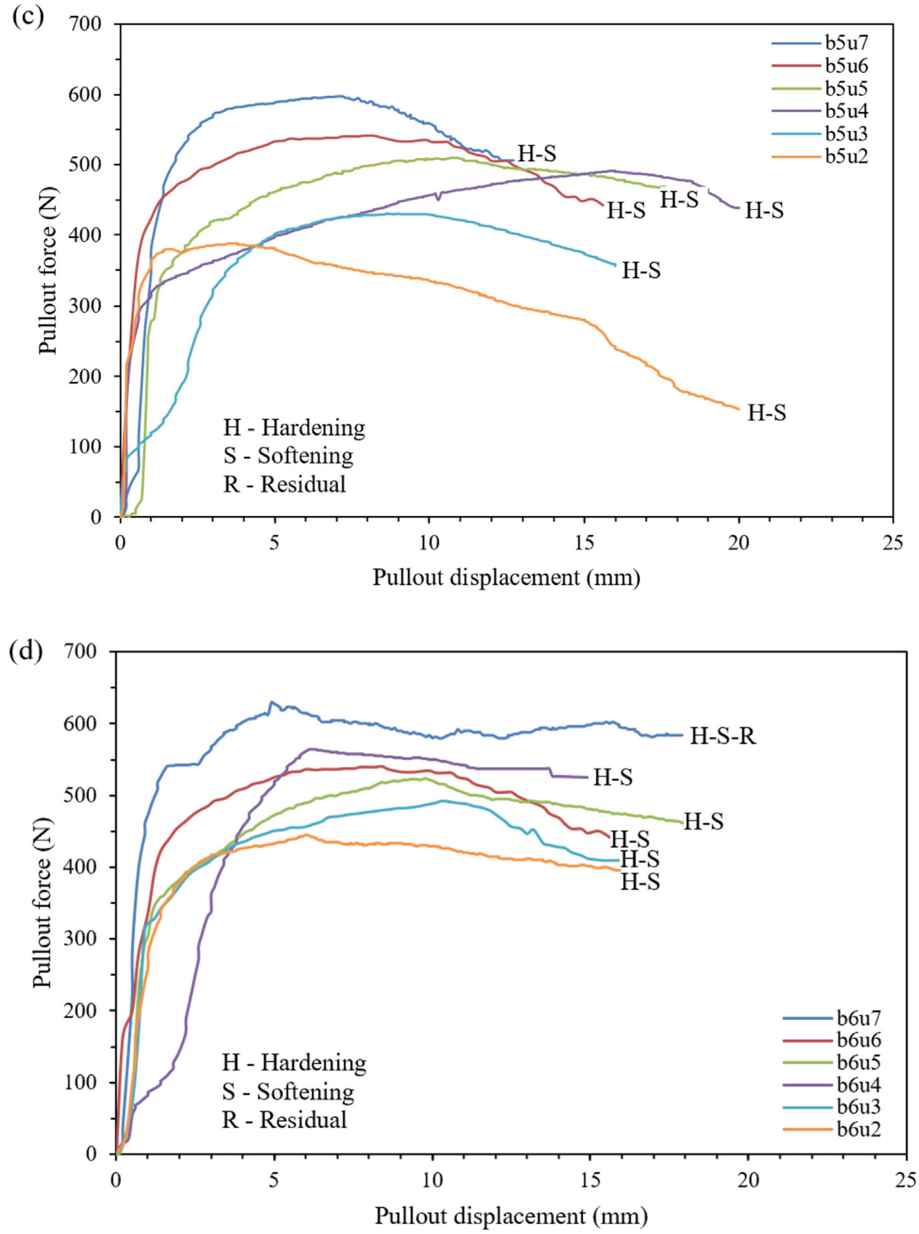

Fig 3. *(continued)*

neighboring slope change in Fig. 6. Specifically, for the specimen groups with the u/b smaller than 1, the greater softening rate (indicated by shadow zone with the value of 15.0 in Fig. 6) can be obviously observed comparing with that with the u/b greater than 1 (e.g., specimens b3u2 versus b3u4, b4u3 versus b4u6, b6u3 versus b6u7). In the limit case, when the softening rate reduces to zero, the softening phase would transfer to the residual phase (e.g., specimens b3u5, b6u7). Although the bound value can be used to distinguish the general trend of the softening rate, the significant nonlinearity between the softening rate and the u/b can be observed, which makes it difficult to find a reasonable correlation between the two parameters. Mechanistically, when the free length equals the bond length (u/b $\approx$ 1), the additional radial stress generated by the restrained contraction of the free section reaches a transition point in its distribution along the bond section. For u/b $<$ 1, the free section is relatively short and this radial stress primarily influences the near end of the bond section, making the interface strength sensitive to changes in u/b. When u/b $>$ 1, the radial stress can no longer proportionally enhance the average strength of the entire bond section, resulting in a slower strength increase and a transition in the post-peak softening mode. It should be noted that this threshold was identified from the specific clay tested in this study, and its precise value may depend on soil properties such as modulus, Poisson's ratio, and interface dilatancy characteristics. Its applicability to other soil types requires further verification.

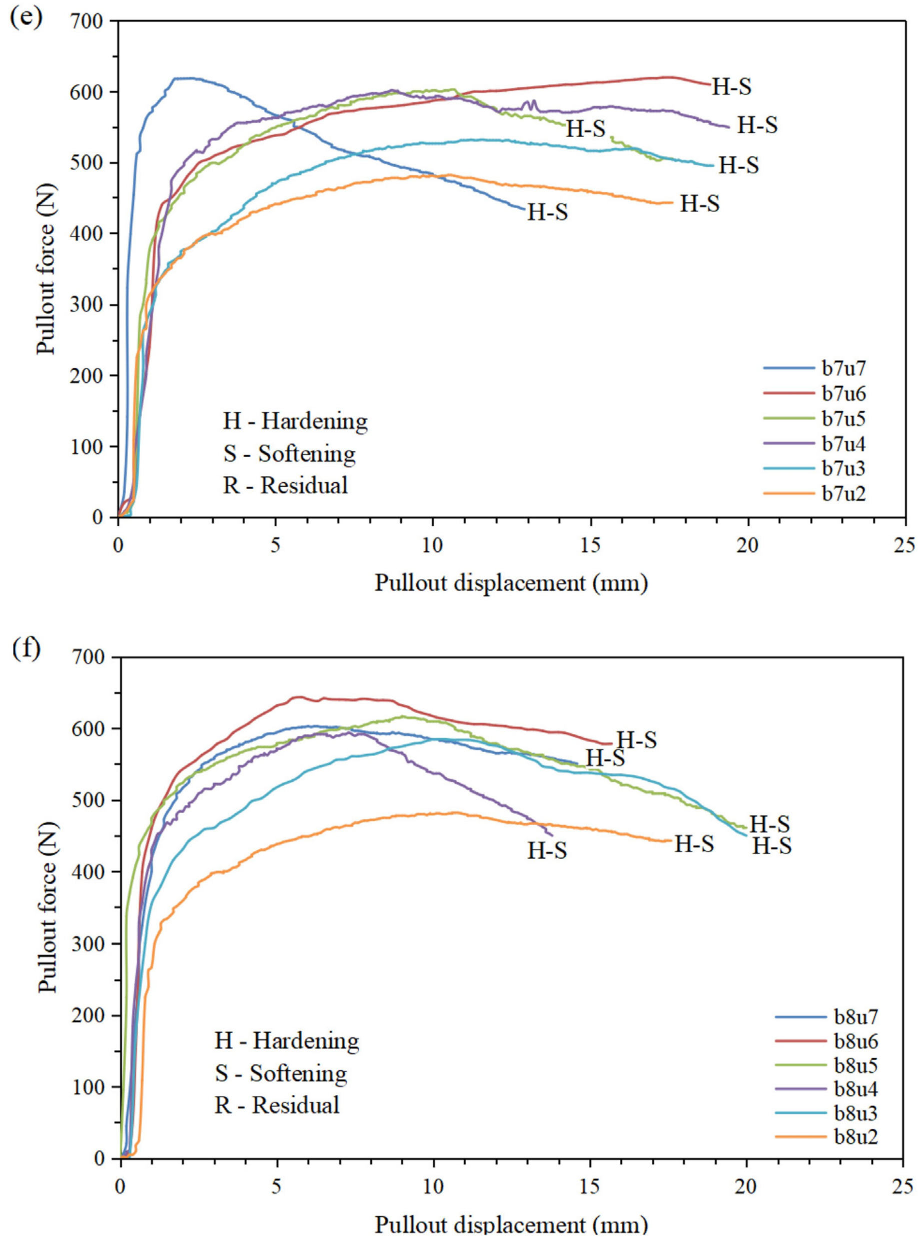

Fig 3. *(continued)*

The bound value for the u/b can also explain why the difference of softening rate for specimens in Fig. 3e–h is much greater than that in Fig. 3a–d. The maximum free length used in the testing program is 7 cm, the free/bond length ratio of specimens in Fig. 3d–h (corresponding to bond length 7–10 cm) is almost smaller than the bound value (seen in Fig. 6e–h). The effect induced by the bound value of the u/b can also be remarkably validated in the comparison between the pullout responses of specimens b6u7 (in Fig. 3d) and b7u7 (in Fig. 3d). The variation of 1 cm at bond length between two specimens leads to a significant change of softening rate in pullout response (transfer from H-S-R to H-S).

3.3. Peak average interface shear strengths

In interface characterization of ground anchor, the peak interface shear strength is the most concerned design parameter as it dictates the pullout resistance of an anchor. The peak and residual pullout forces were used to calculate the corresponding average interface shear strengths (shown in Table 3) by distributing the pullout force over the interface area (i.e., the cylindrical area defined by the diameter of the grouting hole and the length of the bond section). Fig. 7 presents the change of peak average interface shear strength versus the bond length for specimen groups with the same free length.

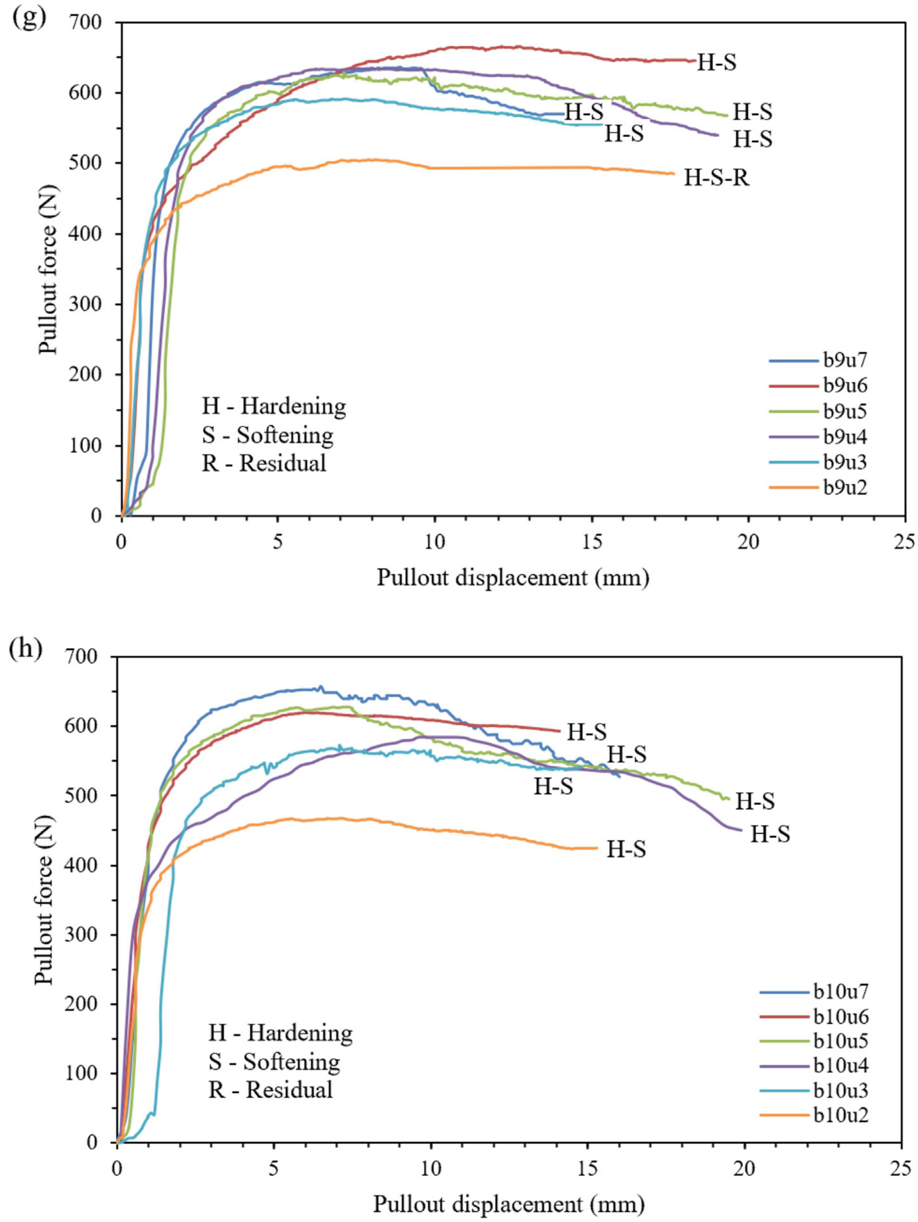

Fig 3. *(continued)*

As shown in Fig. 7, the peak average interface shear strength was found to decrease linearly with increasing bond length. Similar to the influence of free length, this can also be attributed to the soil confinement difference induced by the increasing length of bond section (Fig. 1). The bond length induced influence was measured by the slope of the fitting function seen in Fig. 7. It is found that the increasing free length intensifies the bond length induced decrease of peak average interface shear (slope increasing from 4.84 to 11.13). The slightest decrease (slope of 4.84) can be observed for the specimen group with free length of 2 cm (i.e., of 0.53 normalized to grouting hole diameter). This minimum slope indicates that the sensitivity of peak strength to bond length variation is relatively low under this configuration, and therefore this normalized free length can serve as an empirical reference threshold under the present test conditions.

With respect to the interface shear of soil anchor, it is reported that the shear essentially occurs in the soils adjacent to the interface (Zhang et al., 2020), and the zone with shear deformation is defined as shear band. Hence, the interface shear strength for the soil anchor is obviously relevant to the soil shear strength. In addition, the soil shear strength is constituted of the confinement-free cohesion, and the confinement-dependent friction. As the interface of soil anchor is free of confinement after drilling the anchor hole, the interface shear strength can be straightforward normalized with respect to the soil cohesion. Thus, the peak interface shear strength of soil anchor normalized to the soil cohesion as shown in Table 1 was obtained,

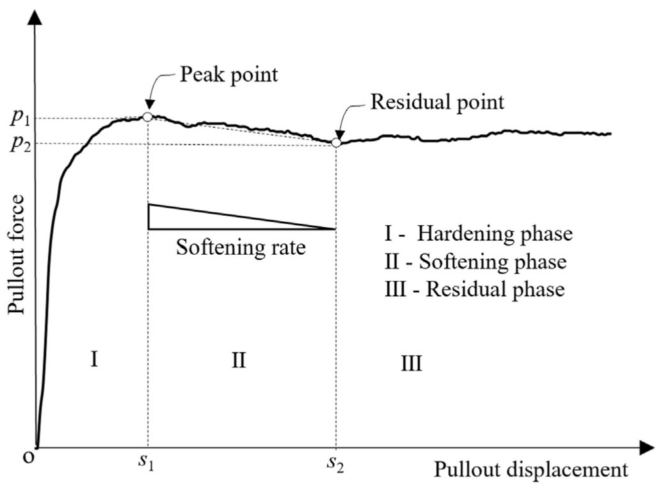

Fig. 4. Schematic of typical characteristic points identified in pullout response.

which was denoted by τ_N. In addition, the u/b was used to represent the combined influence of bond and free length observed in Fig. 7. Thus, the relationship of the τ_N and the u/b was illustrated in Fig. 8.

It is found that the τ_N develops in a linear pattern within a band (i.e., the shadow zone) over the increasing u/b as shown in Fig. 8. The physical mechanism underlying this linear relationship can be explained as follows. During pullout, the soil in the free-section zone is progressively compacted until the initial gap between the grout and the surrounding soil is closed. Once contact is established, further radial contraction of the tensioned free section is resisted, generating additional radial compressive stress at the interface. This stress is transmitted to the bond-section interface, increasing the normal stress acting on it. A longer free section involves a greater volume of compacted soil and thus a larger total confining force, while a longer bond section distributes this force more thinly along the interface. As a result, the average normal stress increment becomes approximately proportional to u/b. According to the Mohr–Coulomb criterion, the frictional component increases linearly with normal stress; consequently, τ_N increases linearly with u/b.

The finding indicates that the influence of soil confinement induced by the difference between the free and bond sections of the element anchor specimen on the interface characterization results can be quantitatively calibrated in processing the testing results. Additionally, the observations on the intersections of the bounds for the linear band (the value of 1.00 for the lower bound and 2.20 for the upper bound) can be used to derive the essential range of the peak interface shear strength tested from the specific interface characterization as the influence of the u/b is eliminated at the value of zero. It should be noted that the intersection of the lower bound observed at the value of 1.00 indicates that the soil cohesion could be the basic source of the interface shear strength as the normal confinement of the interface was released fully in hole drilling. It should also be noted that this linear trend is valid within the tested u/b range of 0.20–2.33, and direct extrapolation beyond this range is not recommended; factors such as specimen alignment deviation and soil density variation may also cause actual results to deviate from this linear band.

4. Numerical modeling of anchor elements

Based on the previously mentioned element concept in laboratory testing of geotechnical materials, the interface bond-slip model of an anchor was directly characterized by the relationship between interface shear stress and interface shear displacement. However, different configuration conditions of element anchor specimens result in varying size and boundary effects, leading to observable differences in pullout response and peak interface shear strength. Consequently, numerical modeling of a pullout test for a typical element anchor specimen was carried out using the FLAC^{3D} (Itasca Consulting Group, 2016) to further investigate the influence of specimen configuration conditions. It should be noted that the cable or pile element (either is from terminology in FLAC^{3D}, as an optional type of structural elements) is commonly adopted in the numerical modelling of soil anchor using FLAC^{3D} due to their concise definition of model parameters. The pile element distinguished with the cable element by the ability of considering the anchorage stiffness and the specific interface bond-slip behavior. As the interface shear (i.e., bond-slip) behavior of soil anchor was straightforwardly obtained from the pullout test of element anchor specimen in this work, the pile element was adopted specially in numerical modelling aiming to implement the customization of interface behavior using the tested results.

Specifically, the straining behavior of the surrounding soils, pullout response and the influence of the method used to maintain a consistent interface contact area were monitored.

4.1. Establishment of the numerical model

The soils surrounding the element anchor specimen were modeled using general grids while the pile structural elements served as the anchorage. As depicted in Fig. 9, the free section of the specimen was simulated by specifying free attachment conditions for links of pile elements. As the shear strength indices of the soils for the tested element anchor specimen were determined using quick direct shear test, the surrounding soils in the numerical model are assumed to comply with the Mohr-Coulomb behavior throughout pullout loading without considering the consolidation. The node of the tendon head was fixed. Aiming to eliminate the loading rate dependency in the numerical modelling, the grids for the upper face of the surrounding soils exerted a downward velocity of 1.67e-5 m/sec, corresponding to the test pullout rate of 1.0 mm/min.

Table 3
Information derived from pullout responses of each element anchor specimen.

b	u	u/b	Peak			Residual			Softening rate
			P_1	t_1	S_1	P_2	t_2	S_2	
cm	cm		N	kPa	mm	N	kPa	mm	N/mm
3	2	0.667	265.87	74.23	9	120.94	33.77	16.1	20.41
	3	1.000	300.85	84.00	7.4	167.92	46.89	16	15.46
	4	1.333	316.19	88.29	7.6	269.66	75.30	19.5	3.91
	5	1.667	336.05	93.83	4.1	306.84	85.68	10.4	4.64
	6	2.000	369.81	103.26	10.3	306.57	85.60	16	11.10
	7	2.333	481.76	134.52	10.5	441.78	123.35	17.1	6.06
4	2	0.500	331.83	69.49	8.5	273.56	57.29	16	7.77
	3	0.750	384.81	80.58	7.3	135.93	28.47	19.9	19.75
	4	1.000	412.79	86.44	2.3	172.80	36.19	20	13.56
	5	1.250	451.77	94.61	10.6	320.84	67.19	16	24.25
	6	1.500	516.74	108.21	12.2	438.78	91.89	20	10.00
	7	1.750	524.73	109.89	5.6	420.79	88.12	19.9	7.27
5	2	0.400	388.06	65.01	3.5	153.57	25.73	20	14.21
	3	0.600	430.78	72.17	8.6	356.31	59.69	16	10.06
	4	0.800	490.75	82.22	15.8	438.41	73.45	19.9	12.77
	5	1.000	509.17	85.30	10.7	466.92	78.22	17.4	6.31
	6	1.200	540.73	90.59	7.9	441.78	74.01	15.6	12.85
	7	1.400	597.70	100.13	7	506.48	84.85	12.3	17.21
6	2	0.333	444.77	62.09	6	394.07	55.02	16	5.07
	3	0.500	491.75	68.65	10.3	407.65	56.91	16	14.75
	4	0.667	563.71	78.70	6.1	524.86	73.27	14.9	4.42
	5	0.833	524.13	73.17	9.8	462.22	64.53	17.9	7.64
	6	1.000	540.73	75.49	8.4	441.78	61.68	15.6	13.74
	7	1.167	629.15	87.84	4.9	579.56	80.91	10.2	9.36
7	2	0.286	481.76	57.65	10.5	441.78	52.87	17.1	6.06
	3	0.429	531.71	63.63	11.2	495.13	59.25	18.7	4.88
	4	0.571	601.75	72.01	8.7	549.24	65.72	19.4	4.91
	5	0.714	602.70	72.12	10.6	502.66	60.15	17.1	15.39
	6	0.857	619.69	74.16	17.3	609.69	72.96	18.8	6.66
	7	1.000	618.39	74.00	2.3	433.48	51.87	12.9	17.44
8	2	0.250	481.76	50.44	10.6	441.78	46.26	17.3	5.97
	3	0.375	584.70	61.22	10.1	449.77	47.09	20	13.63
	4	0.500	593.95	62.19	7.3	449.77	47.09	13.8	22.18
	5	0.625	616.69	64.57	9	460.77	48.25	19.9	14.30
	6	0.750	643.37	67.37	5.8	578.27	60.55	15.4	6.78
	7	0.875	602.69	63.11	6	550.49	57.64	14.6	6.07
9	2	0.222	504.74	46.98	7.9	484.75	45.12	17.4	2.10
	3	0.333	591.80	55.08	6.7	554.70	51.63	14.5	4.76
	4	0.444	635.68	59.16	8	540.54	50.31	18.9	8.73
	5	0.556	629.68	58.61	7.1	567.79	52.85	19.2	5.12
	6	0.667	666.24	62.01	12.1	645.08	60.04	16.7	4.60
	7	0.778	635.82	59.18	8.9	567.62	52.83	13.3	15.50

10	2	0.200	467.76	39.18	6.7	423.78	35.50	14.5	5.64
	3	0.300	572.71	47.97	7.1	537.10	44.99	14.3	4.95
	4	0.400	583.70	48.89	9.6	449.77	37.68	19.9	13.00
	5	0.500	627.68	52.58	6.9	495.24	41.48	19.3	10.68
	6	0.600	619.69	51.91	6	592.85	49.66	14.1	3.31
	7	0.700	657.91	55.11	6.5	527.72	44.21	16	13.70

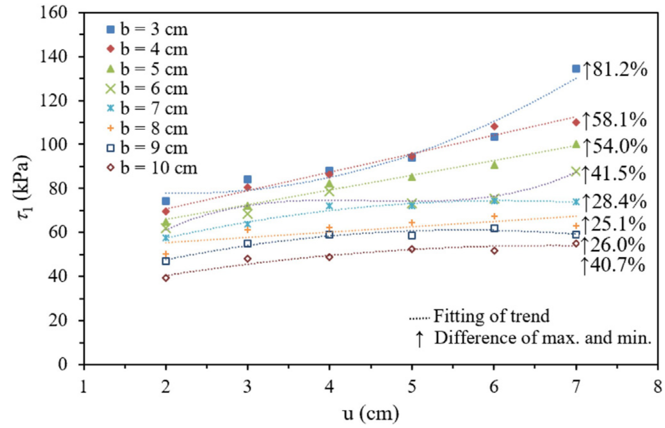

Fig. 5. Peak average interface shear strength versus the free length of the specimen.

The interface shear behavior between the pile element and soil grid was simulated by a shear coupling spring, characterized by interface shear stiffness (‘cs_sk’), and a slider, characterized by interface shear strength (‘cs_scoh’), as shown in Fig. 9.

Using specimen b10u5 as a representative case, the ‘cs_sctable’ command specified with the pile element was used to achieve the customized input of the interface bond-slip model. Specifically, the governing parameter of the slider in Fig. 9 (i.e., ‘cs-scoh’) was customized by an input array of cohesion-displacement pairs, which were essentially the data points of the obtained interface bond-slip curves. Correspondingly, the interface bond-slip model was derived based on the pullout response of specimen b10u5 (Fig. 3h). Specimen b10u5 (bond length = 10 cm, free length = 5 cm) was selected because its bond length was the longest among all tested configurations, which allows the most complete observation of the stress transfer and deformation distribution along the bond section in the numerical model. Table 4 presents the material properties used in the numerical model.

The numerical model adopts several simplifications consistent with the testing conditions. The loading rate is sufficiently low (1 mm/min) that the entire pullout process can be regarded as quasi-static, rendering rate effects negligible. The soil, compacted at a moisture content of 18% (below the plastic limit of 20.9%), has low saturation, and together with the slow loading, the test can be reasonably approximated as drained shear; hence, pore pressure coupling was not incorporated. These simplifications are specific to the present study and would require re-evaluation under substantially different loading or drainage conditions.

4.2. Verification of numerical modeling

The loading of the specimen in the numerical model was terminated at the calculation step of 2500, corresponding to a pullout displacement of 4.2 cm. It is noteworthy that

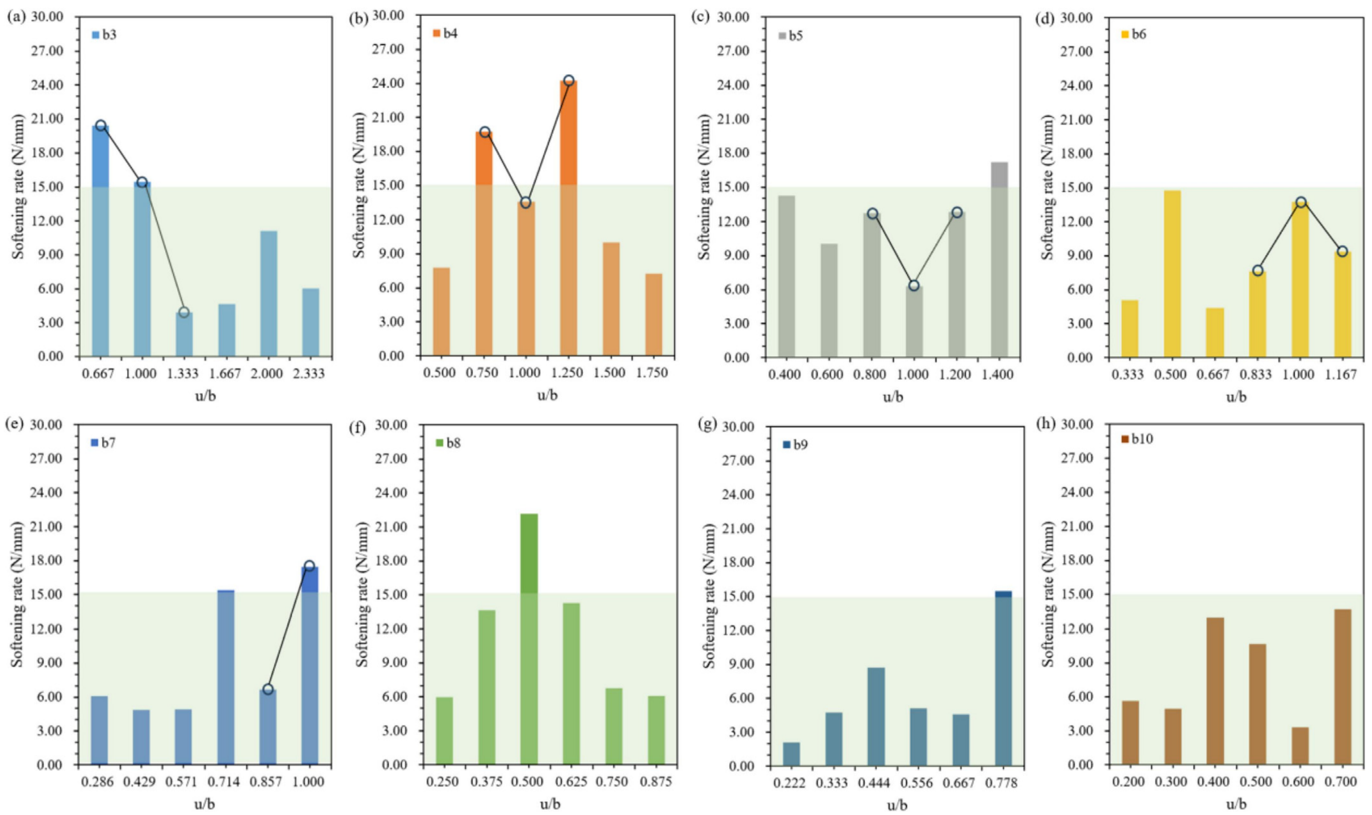

Fig. 6. The softening rate of pullout response versus the free/bond length ratio for specimen groups under different bond lengths: (a) 3 cm; (b) 4 cm; (c) 5 cm; (d) 6 cm; (e) 7 cm; (f) 8 cm; (g) 9 cm; and (h) 10 cm.

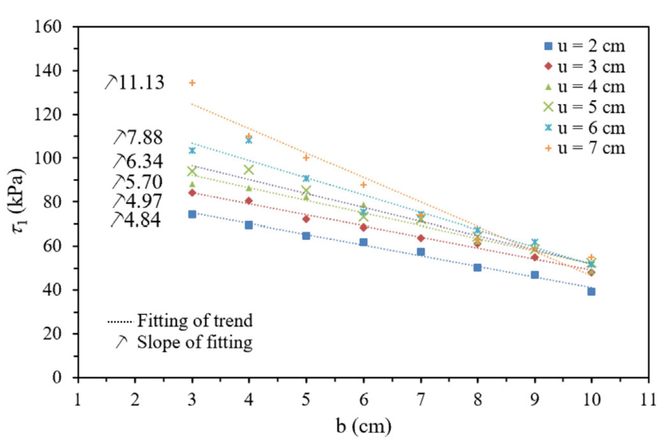

Fig. 7. Peak average interface shear strength versus the bond length of the specimen.

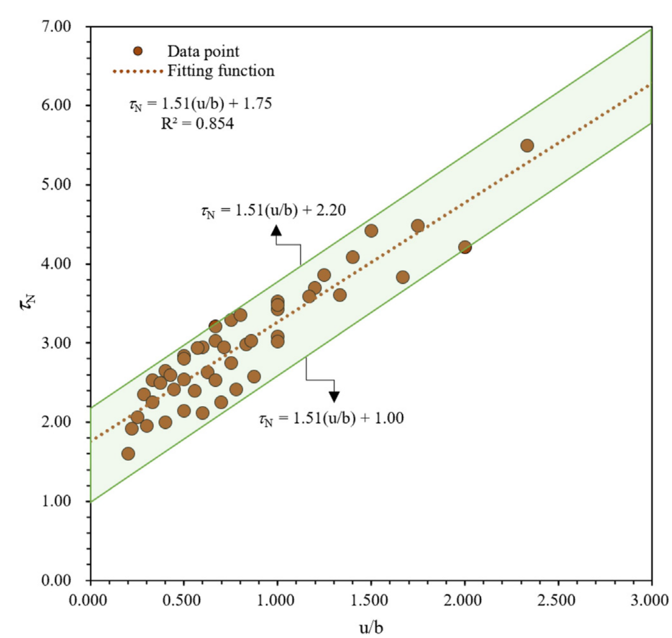

Fig. 8. Normalized peak average interface shear strength versus the free/bond length ratio.

pullout displacement was terminated at 2 cm due to the limited range of the step motor in the laboratory test. An extended pullout displacement range was used in numerical modeling to ensure the interface shear reached the strain softening or residual phase. The unbalanced nodal force at the top of the pile element was monitored as the pullout force throughout the loading process (Itasca Consulting Group, 2016). The pullout response of the numerical model is presented in Fig. 10 along with the shear stress distribution of the surrounding soils upon termination of loading.

As can be observed in the pullout response in Fig. 10, a marginal pullout force was generated at the anchor head, between 0 and 0.5 cm of displacement (range AB), reveal-

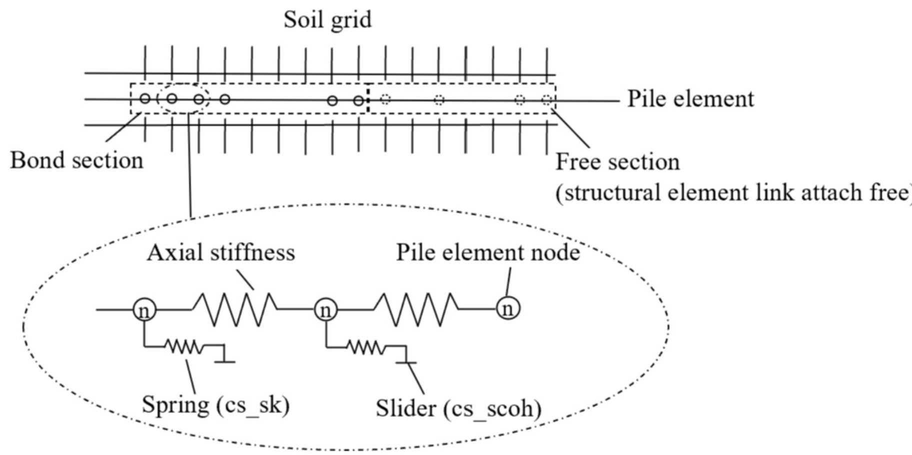

Fig. 9. Schematic of anchor modeled using structural pile element in FLAC^{3D}.

Table 4
Material properties used in numerical model.

Material properties	Value
Cohesion of soil model (kPa)	24.5
Frictional angel of soil model (°)	38.7
Elastic bulk modulus of soil model (MPa)	16
Elastic shear modulus of soil model (MPa)	10
Elastic modulus of anchorage (GPa)	20.0
Poisson's ratio of anchorage	0.25
Anchorage diameter (cm)	3.8
Bond length of the specimen (cm)	10
Free length of the specimen (cm)	5

ing that no interface shear occurred at the bond section of the specimen. This range typically corresponds to the compaction of the surrounding soils in the free section of the specimen. Next, the compacted soil in the free section transferred the shear stress to the interface in the bond section, resulting in interface slip when the shear stress exceeded the interface shear strength (range BC). The interface slip corresponding to the interface shear strength was confirmed by the peak pullout displacement of 1 cm at the anchor head. Thereafter, the interface gradually developed into the strain softening phase (range CD) and the pullout force decreased to its minimum value. The interface strain softening was accompanied by the recovery of elastic defor-

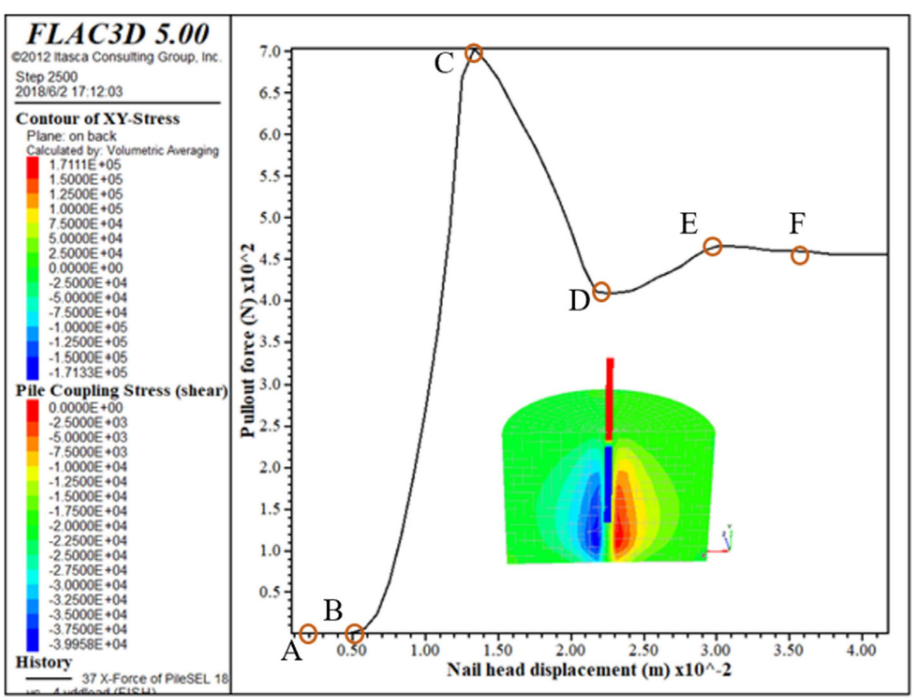

Fig. 10. Pullout response obtained from numerical simulation of specimen b10u5.

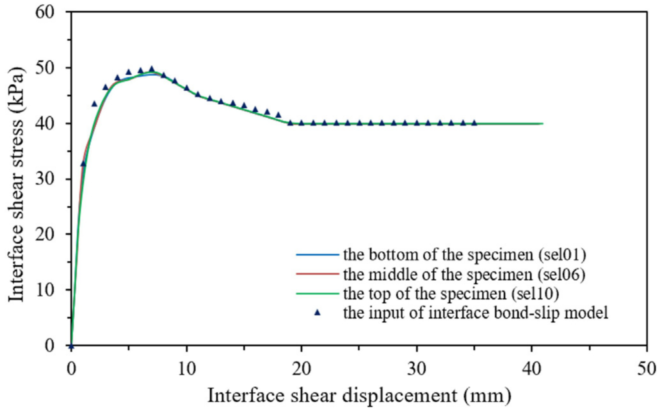

Fig. 11. Comparison of input and histories of interface shear behavior.

mation of the soil at certain interfaces, causing an uplift effect on the anchor demonstrated by the increasing pullout force (range DE). The pullout force remained constant and soil deformation remained stable (range EF).

Additionally, the interface shear stress-displacement histories for three pile elements (sel01, 06 and 10), corresponding to the specimen bottom, middle and top, were obtained for comparison with the interface bond-slip model input as depicted in Fig. 11. Good agreement across all three positions can be observed, thus validating the correspondence of the input interface model in the numerical model and laboratory testing. The good agreement observed at these three positions also confirms that the selection of b10u5 as the calibration baseline is reasonable.

4.3. Numerical prediction of soil deformations

During the pullout loading process, a uniform distribution of interface shear displacement over the bond length can be assumed when the surrounding soils deform uni-

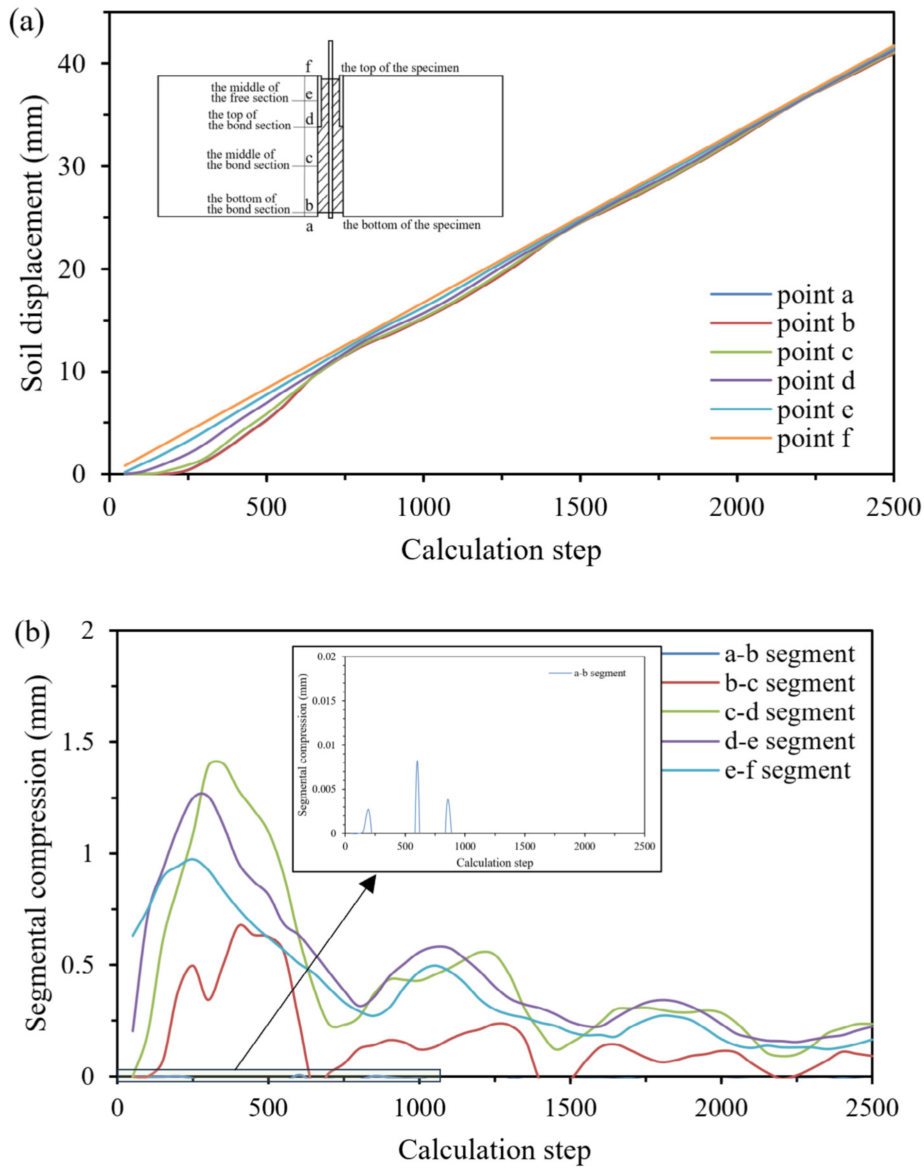

Fig. 12. Soil deformation at various positions along element anchor specimen: (a) displacement; and (b) compression.

formly across the bond section along with increasing pullout displacement. However, it is difficult to achieve these conditions with an element anchor specimen. This is because, from the onset of loading, the surrounding soils at different positions along the specimen undergo changes in density and varying degrees of compaction induced by different soil compressions throughout the loading process. Fig. 12 shows the displacement of the surrounding soils at six different positions along the anchor, including the top of the specimen, middle of the free section, top of the bond section (the boundary between the free and bond sections), middle of the bond section, bottom of the bond section, and bottom of the specimen, as well as the corresponding soil compression between adjacent positions.

As seen in Fig. 12a, the soil displacement at the top of the specimen (point f) increased linearly with an increasing calculation step, corresponding to a loading rate of 1 mm/min at the upper boundary of the specimen. As seen in Fig. 12b, an approximate zero compression for segment a-b can be observed in the closeup range with the maximum lower than 0.01 mm. For the remaining positions (points c-f), the soil displacement gradually decreased from the top of free section (point f) through the bottom of the bond section (point b), indicating an accumulation of soil compression from the bottom (free surface) to the top (loading surface) of the specimen. However, the soil displacement exhibits similar trends at different positions with increasing calculation steps, implying the soil compression shifted to the stable phase.

The soil compression of different segments reached its peak within a loading displacement of 0.85 cm followed by a variable decrease. For different segments of the same soil thickness within the free section, less soil compression was observed farther away from the bond section than closer to the bond section, indicating that the propagation of interface shear stress in the surrounding soils effectively enhanced soil compression. Furthermore, the maximum soil compression occurred at the boundary of the bond and free sections (segments c-d and d-e), indicating the interface shear stress could concentrate at the free/bond transfer zone. Additionally, the soil compression of segments within the bond section (segments b-c and c-d) was greater than that in the free section (segments d-e and e-f); and within the bond section, the soil compression in the segment near the bottom (segment b-c) was less than that near the top (segment e-f); these observations indicate that the interface shear stress decreased from the bottom (free surface) to the top (loading surface) of the specimen. It is noteworthy that the soil compression of all segments decreased overall with increasing loading displacements, but with rebounds in certain sections. A maximum rebound was reached at a loading displacement of 2.1 cm, corresponding to the rebound of the pullout force from the trough to the stable phase (point D to point E in Fig. 10).

Fig. 13 depicts the strain distribution of the surrounding soils at different stages of the pullout response (Fig. 10). Soil deformation mainly occurred around the free section

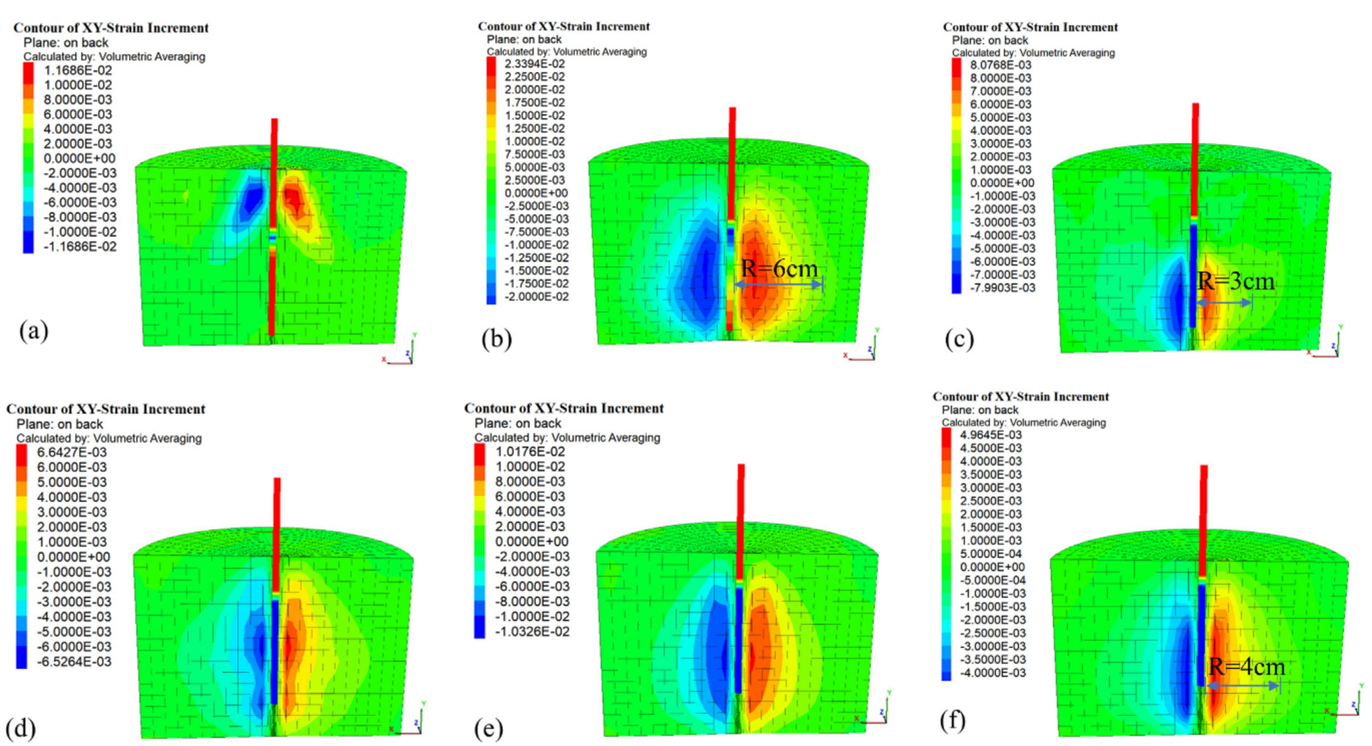

Fig. 13. Soil strain distribution for different stages of pullout response in Fig. 6: (a) point A – 1.67 mm; (b) point B – 5.01 mm; (c) point C – 14.20 mm; (d) point D – 22.55 mm; (e) point E – 30.06 mm; and (f) point F – 35.07 mm.

in the early stages of displacement loading (Fig. 13a). Furthermore, soil compression developed toward the bond section, indicating the initialization of interface shear (Fig. 13b). Next, the area of soil deformation near the interface reduced significantly. Here, the radius of interface shear influence is defined as the maximum radial extent within which identifiable shear deformation occurs in the surrounding soil; its specific values can be quantitatively extracted from the numerical output files. Based on this definition, the maximum radius of the interface shear influence area decreased, from 6 cm at initialization to 3 cm at the peak pullout force (Fig. 13c), stabilizing at around 4 cm (Fig. 13e and f). It should be noted that these values were obtained from the specific clay and anchor diameter adopted in this study; the reproducibility of this radius under different soil types or anchor diameters remains to be verified through further investigation.

At the stage corresponding to the peak pullout force, a spindle-shaped distribution was observed along the bond length. At the stage corresponding to the minimum pullout force, an inconsistent distribution of soil deformation was observed along with a discontinuous local strain concentration and partial rebound (Fig. 13d). At the stage corresponding to the residual pullout force, a nearly uniform distribution of soil deformation over the bond length (Fig. 13f) was observed near the interface.

Because the anchorage deformation was negligible due to its large axial stiffness, the soil deformation distribution represents the interface shear displacement distribution. It can be concluded that the uniformity of the interface shear displacement distribution under the residual pullout force was greater than that under the peak pullout force, while both exceeded that under the minimum pullout force.

It is noteworthy that the soil deformation near the interface caused a change in the distribution of shear interface displacement and that the consistency of the shear stress distribution along the interface also varied according to the interface bond-slip model (Fig. 11). Additionally, soil deformation could have induced the variation in soil density of the specimen. While the initial compactness was due to conditioning in specimen preparation to achieve a uniform density distribution, varying soil compression at different positions was observed during the pullout loading procedure (Fig. 12). It has previously been reported that interface shear behavior can be affected by the soil density of an element anchor specimen (Zhang et al., 2020) and an optimized interface bond-slip model accounting for the coupled effect between soil compression and soil density is greatly needed for an effective simulation and prediction of the pullout response. In the present model, however, such density variations and their effect on the interface response were not taken into account. Because the accumulated soil compression prior to and around the peak is relatively small, neglecting these variations has little influence on the simulated peak and softening stages. The residual stage, where more pronounced compression and rebound may develop locally, is more likely to be affected.

4.4. Comparison of two methods ensuring constant specimen interface area

Two methods can be used to ensure a constant interface contact area of the element anchor specimen: the reserved soil method and the reserved anchorage method. The reserved soil method is implemented by establishing a free section at the front of the bond section in the pullout direction (Fig. 14a), while the reserved anchorage method is implemented by creating a reserve anchorage at the rear of the bond section in the pullout direction (Fig. 14b).

Using specimen b10u5 as a typical example, element anchor specimens were prepared via the two methods previously described, and both were numerically modelled based on the same material properties, loading strategy and interface model discussed in section 4.1. A comparison of the pullout responses of element anchor specimens for the two methods is shown in Fig. 15.

As Fig. 15 demonstrates, the two methods produce very different effects on the pullout response of an element anchor specimen. Compared with the reserved soil method, a 6.5% decrease in peak pullout force and 5.2% increase in residual pullout force were observed with the reserved anchorage method. This discrepancy can be attributed to the occurrence of rebound soil deformation seen with the reserved soil method, which is revealed in the pullout response by the rebound from the trough of the pullout force. Specifically, this rebound pullout force was mainly

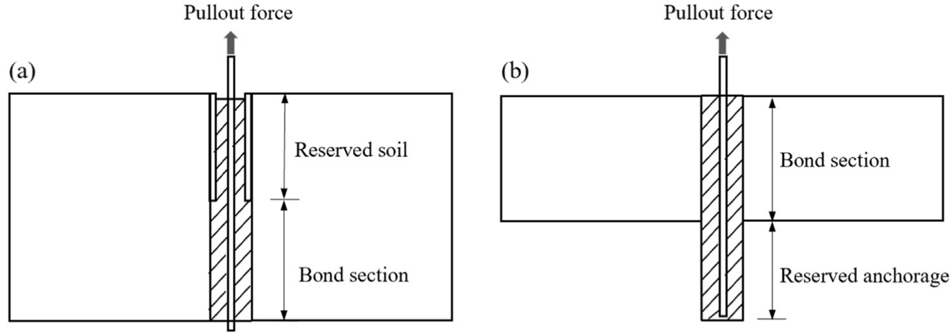

Fig. 14. Two methods to ensure constant anchor interface area: (a) reserved soil method; and (b) reserved anchorage method.

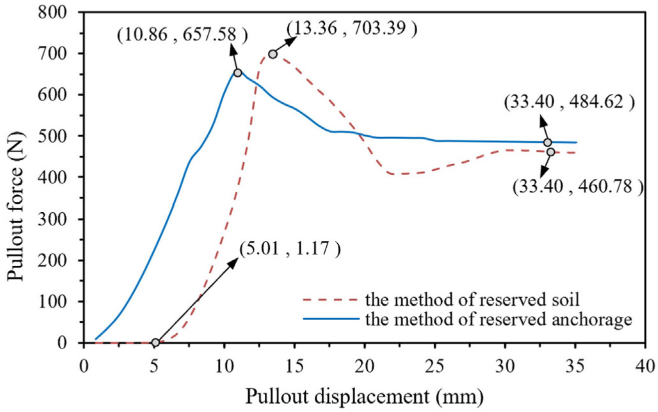

Fig. 15. Comparison of specimen pullout responses for reserved soil and reserved anchorage methods.

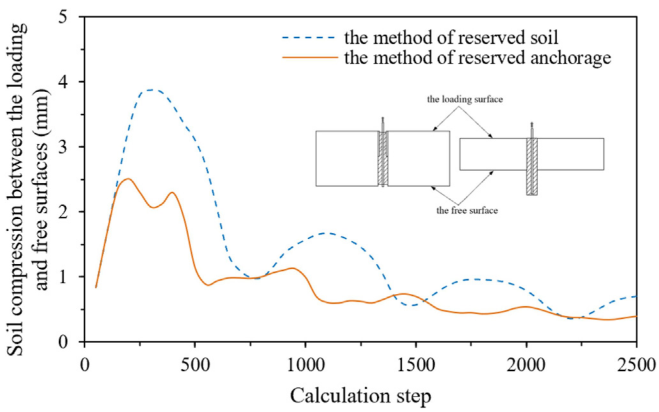

Fig. 16. Specimen soil compression for reserved soil and reserved anchorage methods.

caused by the compression of reserved soil prior to the initialization of interface shear, which corresponds to the development of pullout force until a pullout displacement of 5 mm was reached.

Fig. 16 compares the variation in soil compression between the loading and free surfaces for the reserved soil and reserved anchorage methods. The reserved soil method led to an increased rebound of soil deformation, peaking at 30% of the maximum soil compression. In contrast, the reserved anchorage method yielded negligible soil rebound throughout the pullout loading process. Since the soil compression dictates the interface shear displacement, the reserved anchorage method is recommended for element anchor specimen preparation, as it eliminates the soil rebound effect and achieves a more uniform distribution of shear displacement along the interface. In field practice, this method is preferentially recommended for deformation-sensitive projects where construction conditions permit, while the reserved soil method remains a viable option for conventional applications.

5. Conclusions

This study explores the influence of the configuration conditions of element anchor specimens on the characterization of an anchorage interface. Pullout tests were carried out on 48 sets of element anchor specimens with different bond/free length ratios. The effects of soil deformation and methods to ensure a constant interface contact area were analyzed using numerical simulations. Based on the results obtained, the following conclusions were drawn:

(1) The free/bond length ratio of the specimens was found to significantly influence the interface characterization results. The softening rate of the pullout response does not constitute a continuous quantitative functional relationship with u/b; however, two distinct softening modes can be significantly distinguished by a bound value of the free/bond length ratio at around 1. The normalized peak average ultimate interface shear strength linearly increased with the free/bond length ratio at least within the tested free/bond length range used in this work.
(2) Size effect of element anchor specimens is obviously observed. To minimize the effects of different configuration conditions on interface strength, an element anchor specimen with a combination of bond length/grout diameter ratio at 2.1 and a free length/grout diameter ratio at 0.52 was suggested.
(3) A numerical model of an element anchor specimen effectively simulated the pullout response in laboratory tests. The radius of the interface shear influence area decreased gradually after the initialization of interface shear. The influence area exhibited a spindle-shaped distribution in the peak pullout phase, while a uniform distribution over the length of the interface was observed in the residual phase.
(4) To ensure a constant interface contact area of the element anchor specimen in interface characterization, the reserved soil method increased the rebound effect of soil deformation, peaking at 30% of the maximum soil compression; however, the reserved anchorage method led to negligible rebound throughout the loading process and achieved a more uniform distribution of interface shear displacement. The reserved anchorage method was therefore suggested for element anchor specimen preparation. In field practice, this method is preferentially recommended for deformation-sensitive projects where construction conditions permit, while the reserved soil method remains a viable option for conventional applications.

It should be noted that this study was conducted using element-scale specimens on a single clay type under zero-confinement conditions. The quantitative thresholds identified and the linear τ_N–u/b relationship are therefore empirical in nature, and their generalizability to other soil types or stress states requires further verification. The numerical model was calibrated against a single specimen and serves primarily as a mechanistic interpretation tool; systematic multi-configuration validation remains a future task. The description of the shear deformation zone is qualitative, and quantitative characterization of the shear band was not performed. Extrapolation of the element-scale findings to field-scale anchors follows a load-transfer analysis framework, which still requires validation through full-scale field pullout tests. Future work will extend the tests to other soil types, pursue quantitative shear band characterization, incorporate systematic numerical validation, and develop a more complete theoretical framework.

CRediT authorship contribution statement

Genbao Zhang: Writing – review & editing, Supervision, Resources, Funding acquisition, Conceptualization. **Tianchong Feng:** Writing – review & editing, Writing – original draft, Investigation. **Jorge G. Zornberg:** Writing – review & editing. **Changfu Chen:** Writing – review & editing, Supervision, Resources, Conceptualization. **Haibin Ding:** Writing – review & editing, Writing – original draft. **Junbo Sun:** Writing – review & editing, Writing – original draft. **Shimin Zhu:** Writing – review & editing, Investigation. **Changjie Xu:** Writing – review & editing, Supervision, Resources, Funding acquisition.

Acknowledgments

This work was sponsored by National Key R & D Program of China (Grant number: 2023YFC3009400), National Natural Science Foundation of China (Grant numbers: 52578400), Natural Science Foundation of Hunan Province (Grant number: 2025JJ50294). The authors appreciate their supports.

References

Benmokrane, B., Chennouf, A., Mitri, H.S., 1995. "Laboratory evaluation of cement-based grouts and grouted rock anchors. Int. J. Rock Mech. Min. Sci. Geomech. Abstracts 32 (7), 633–642. https://doi.org/10.1016/0148-9062(95)00021-8.

Chen, C.F., Zhu, S.M., Zhang, G.B., Morsy, A.M., Zornberg, J.G., Huang, J.B., 2022a. Interface creep behavior of tensioned GFRP tendons embedded in cemented soils. Geosynth. Int. 29 (3), 241–253. https://doi.org/10.1680/jgein.21.00008.

Chen, C.F., Zhu, S.M., Zhang, G.B., Mao, F.S., Cai, H., 2021. Time-dependent load transfer behavior of grouted anchors in laterite. Comput. Geotech. 132. https://doi.org/10.1016/j.compgeo.2020.103969 103969.

Chen, C.F., Zhu, S.M., Zhang, G.B., Morsy, A.M., Zornberg, J.G., Mao, F.S., 2022b. A generalized load-transfer modeling framework for tensioned anchors integrating adhesion–friction-based interface model. Int. J. Geomech. 22 (5). https://doi.org/10.1061/(ASCE)GM.1943-5622.0002338 04022036.

Chen, C.F., Zhang, G.B., Zornberg, J.G., Morsy, A.M., Huang, J.B., 2020. Interface bond behavior of tensioned glass fiber-reinforced polymer (GFRP) tendons embedded in cemented soils. Constr. Build. Mater. 263. https://doi.org/10.1016/j.conbuildmat.2020.120132 120132.

Chen, C.F., Zhu, S.M., 2024. Element-scale pullout test study on the mechanical behavior of grouted anchor–soil interface subjected to ground pressure. Acta Geotech. 19 (8), 5433–5447. https://doi.org/10.1007/s11440-024-02256-5.

Chen, C.F., Zhang, G.B., Zornberg, J.G., Morsy, A.M., Zhu, S.M., Zhao, H.B., 2018. Interface behavior of tensioned bars embedded in cement-soil mixtures. Constr. Build. Mater. 186, 840–853. https://doi.org/10.1016/j.conbuildmat.2018.07.211.

Chen, C.F., Zhang, G.B., Zornberg, J.G., Zheng, X.X., 2019. Element nail pullout tests for prediction of soil nail pullout resistance in expansive clays. Geotech. Test. J. 42 (5), 1274–1297. https://doi.org/10.1520/GTJ20170431.

Cheng, Y.M., Au, S.K., Yeung, A.T., 2016. Laboratory and field evaluation of several types of soil nails for different geological conditions. Can. Geotech. J. 53 (4), 634–645. https://doi.org/10.1139/cgj-2015-0267.

Chen, Y., Zhang, R., Zi, J., et al., 2025. Evaluation of the treatment variables on the shear strength of loess treated by microbial induced carbonate precipitation. J. Mt. Sci. 22, 1075–1086. https://doi.org/10.1007/s11629-024-9100-3.

GB50086-2015. 2016. Technical code for engineering of ground anchorages and shotcrete support. China Planning Press, Beijing, China.

Han, J., Liu, D., Guan, Y., Chen, Y., Li, T., Jia, D., Yan, F., Jia, P., Zhao, Y., 2022. Study on shear behavior and damage constitutive model of tendon-grout interface. Constr. Build. Mater. 320. https://doi.org/10.1016/j.conbuildmat.2021.126223 126223.

Itasca Consulting Group, 2016. PFC 5.0 documentation. Itasca Consulting Group, Minneapolis, MN.

Li, T., Zhao, W., Liu, R., Han, J., Jia, P., Cheng, C., 2024. Visualized direct shear test of the interface between gravelly sand and concrete pipe. Can. Geotech. J. 61 (2), 361–374. https://doi.org/10.1139/cgj-2022-0007.

Li, Z., Lin, W., Ye, J., Chen, Y., Bian, X., Gao, F., 2021. Soil movement mechanism associated with arching effect in a multi-strutted excavation in soft clay. Tunn. Undergr. Space Technol. 110. https://doi.org/10.1016/j.tust.2021.103816.

Liu, J., Qu, K., Ding, W., et al., 2022. Evolution analysis of pressure-arch of deeply buried horseshoe tunnel in hard plastic silty clay layers. Yangtze River 53 (1), 189–197. https://doi.org/10.16232/j.cnki.1001-4179.2022.01.029.

Liu, X.M., Wang, J.Q., Huang, J., Jiang, H.W., 2017. Full-scale pullout tests and analyses of ground anchors in rocks under ultimate load conditions. Eng. Geol. 228, 1–10. https://doi.org/10.1016/j.enggeo.2017.07.004.

Ma, S.Q., Zhao, Z.Y., Nie, W., Gui, Y.L., 2016. A numerical model of fully grouted bolts considering the tri-linear shear bond–slip model. Tunn. Undergr. Space Technol. 54, 73–80. https://doi.org/10.1016/j.tust.2016.01.033.

Martin, L.B., Tijani, M., Hadj-Hassen, F., 2011. A new analytical solution to the mechanical behaviour of fully grouted rockbolts subjected to pull-out tests. Constr. Build. Mater. 25 (2), 749–755. https://doi.org/10.1016/j.conbuildmat.2010.07.011.

Ren, F.F., Yang, Z.J., Chen, J.F., Chen, W.W., 2010. An analytical analysis of the full-range behaviour of grouted rockbolts based on a tri-linear bond-slip model. Constr. Build. Mater. 24 (3), 361–370. https://doi.org/10.1016/j.conbuildmat.2009.08.021.

Wang, J., Wu, X., Qin, W., et al., 2023. Negative skin friction of piles installed in dredged slurry after being reinforced by the vacuum preloading method. Acta Geotech. 18 (11), 16. https://doi.org/10.1007/s11440-023-01998-y.

Zhang, G.B., Chen, C.F., Li, K.F., Xiao, F., Sun, J.B., Wang, Y.F., Wang, X.Y., 2022a. Multi-objective optimisation design for GFRP tendon reinforced cemented soil. Constr. Build. Mater. 320. https://doi.org/10.1016/j.conbuildmat.2021.126297 126297.

Zhang, G.B., Chen, C.F., Zhang, Y.H., Zhao, H.C., Wang, Y.F., Wang, X.Y., 2022b. Optimised neural network prediction of interface bond strength for GFRP tendon reinforced cemented soil. Geomech. Eng. 28 (6), 599–611. https://doi.org/10.12989/gae.2022.28.6.599.

Zhang, G.B., Chen, C.F., Zornberg, J.G., Morsy, A.M., Mao, F.S., 2020. Interface creep behavior of grouted anchors in clayey soils: effect of soil moisture condition. Acta Geotech. 15, 2159–2177. https://doi.org/10.1007/s11440-019-00907-6.

Zhang, G.B., Chen, C.F., Sun, J.B., Li, K.F., Xiao, F., Wang, Y.F., Chen, M.C., Huang, J.Z., Wang, X.Y., 2022c. Mixture optimisation for cement-soil mixtures with embedded GFRP tendons. J. Mater. Res. Technol. 18, 611–628. https://doi.org/10.1016/j.jmrt.2022.02.076.

Zhao, X., Liu, Y., Chang, J., et al., 2025. Soil arching evolution and influencing factors of gravel soil slope anchored anti-slide pile based on particle flow simulation. J. Eng. Geol. 33 (1), 356–366. https://doi.org/10.13544/j.cnki.jeg.2022-0845.

Zou, J.F., Zhang, P.H., 2019. Analytical model of fully grouted bolts in pull-out tests and in situ rock masses. Int. J. Rock Mech. Min. Sci. 113, 278–294. https://doi.org/10.1016/j.ijrmms.2018.11.015.

Zhu, S.M., Chen, C.F., Zhang, G.B., Du, C., 2022. Theoretical and experimental investigations of anchoring force loss behavior for prestressed ground anchors. Can. Geotech. J. 59 (9), 1587–1601. https://doi.org/10.1139/cgj-2021-0220.